Nanomed Res J 10(4):430-438, Autumn 2025

RESEARCH ARTICLE

Enhanced Anticancer Therapy Using Magnetic Nanoparticles Synthesized via Laser Ablation and Activated by Laser Irradiation.

Nada S Ahmade* , Olfat A Mahmood*, Rafid M Abdullah

Department of physical, Collage of Science, University of Diyala, Diyala, Iraq.

ARTICLE INFO

Article History:
Received 17 Sep 2025
Accepted 13 Nov 2025
Published 01 Dec 2025

Keywords:
Laser Ablation
Iron Oxide Nanoparticles
Anticancer

ABSTRACT

In recent times, there has been a lot of attention given to iron oxide nanoparticles (IONPs) because of the exceptional physicochemical characteristics, biocompatibility and multi-functional therapeutic properties of this product. In this paper, IONPs have been prepared in aqueous medium through the pulsed laser ablation of an iron target with 300, 400 and 500 mJ power and discussed by X-ray diffraction (XRD) and field emission scanning electron microscopy (FESEM). XRD analysis ensured that the product was highly pure iron oxide with a cubic spinel structure, whereas FESEM showed irregular and agglomerated nanoparticles with a size ranging between 46.71 and 142.6nm and a predominantly spheric to slightly polyhedric morphology, which are indicative of a polydisperse system. Through a crystal violet cytotoxicity assay, the anticancer property of IONPs was compared to the HepG2 cancer cells and RD normal cells. IONPs prepared at 500 mJ had the best growth inhibition in both cell lines and this was due to the higher concentration of nanoparticle, small size and high surface area. Interestingly, it was observed that the cytotoxicity profile caused the selective induction of the apoptosis of cancer cells with relatively reduced impact on the normal cells, thus showing some selectivity. After 5 minutes of radiation of 532 nm laser diode, IONPs produced localized photothermal heating and reactive oxygen species (ROS), resulting in the oxidative stress, mitochondrial damage, and apoptosis in tumor cells. Photodynamic effect coupled with photothermal effect, combined with intrinsic magnetic responsiveness of IONPs, offers a flexible system of spatially controlled and minimally invasive cancer therapy. These results indicate that laser ablation is a clean, controllable route to fabricate magnetic IONPs that would have potential applications in multimodal anticancer therapies.

How to cite this article
Ahmade N.S., Mahmood O.A., Abdullah R.M. Enhanced Anticancer Therapy Using Magnetic Nanoparticles Synthesized via Laser Ablation and Activated by Laser Irradiation.. Nanomed Res J, 2025; 10(4): 430-438. DOI: 10.22034/nmrj.2025.04.010

INTRODUCTION

Laser ablation in liquid (PLAL) is one of the emerging modern environmentally-friendly methods of producing high-purity nanoparticles without any chemical precursors and surfactants [1]. The method is physical and top-down whereby high-intensity pulsed laser beams are directed to a submerged liquid target of solid iron, resulting in rapid heating of surface, melting, and vaporization, which is followed by forming of a plasma plume and ultrafast quenching to produce iron oxide nanostructures [2, 3].

The targets that are normally utilized in this process are pure iron or iron-based alloys and Nd:YAG lasers with a wavelength of 1064 or 355 nm and pulse durations of femtosecond-nanosecond allow the fine tuning of particle formation [4]. The rate of ablation is modulated by laser parameters including pulse energy, wavelength, irradiation time, and the concentration of particles, colloidal stability, and agglomeration degree, and the liquid phase (e.g., water vs. ethanol) has a strong impact on oxidation state and phase composition [5-9].

* Corresponding Author Email: *nadaahmad@uodiyala.edu.iq*

Magnetic nanoparticles (MNPs) and especially IONPs have attracted much interest in the oncology field because of their magnetic properties, biocompatibility and ease of surface functionalization, which allows them to be used in targeted drug delivery, imaging and image-guided therapy [10, 11]. Compared to standard chemotherapy and radiotherapy, which can often be restricted by the systemic contribution of the drug and lack of tumor specificity, MNP-based systems may be utilized in magnetic targeting to tumors, magnetic hyperthermia [12, 13], and ferroptosis-/ROS-mediated programmed cell death, as well as used as contrast agents in magnetic resonance imaging (MRI) and in tumor real-time monitoring [14, 15].

Among the many available synthesis methods, laser ablation in liquid is especially appealing to synthesize iron oxide nanoparticles to be used in biomedical applications due to its simplicity, comprising no templates, no reagents, minimal contamination, and control of particle size, morphology, crystallinity, and magnetic qualities by simply changing laser fluence and exposure conditions. PLAL has high purity, small size distribution, and high reproducibility when compared to the chemical reduction/precipitation techniques, essential to clinical translation [2, 3, 16, 17].

Iron oxide nanoparticles are also the best to be used in laser mediated cancer therapy as they can take up light and convert this into heat and can be used to achieve localized photo-thermal ablation of tumor tissue when exposed to specific wavelengths [18-20]. These nanoparticles can also undergo photodynamic processes under certain conditions, wherein they produce reactive oxygen species (ROS) that induces oxidative stress, mitochondrial dysfunction, and apoptosis, thus, merging photothermal and photodynamic effects on a single platform [20, 21].

In addition, the superparamagnetic characteristics of iron oxide nanoparticles enable them to be accumulated in the tumor sites using external magnetic fields and to be actively targeted when conjugated with tumor-specific ligands or the antibodies [22-24]. The multimodal nanotheranostic approach of magnetic guidance, photothermal heating, ROS-based photodynamic action is expected to provide high level of efficacy, low level of invasiveness and low level of off-target toxicity in the treatment of advanced cancer therapy.

This work aims to synthesize IONPs via pulsed laser ablation in liquid using varying energies (300, 400, and 500 mJ) on an iron target in double-distilled water, characterize their structural, morphological, magnetic, and optical properties using XRD, FESEM, VSM, and UV-Vis spectroscopy, and evaluate their selective anticancer efficacy against

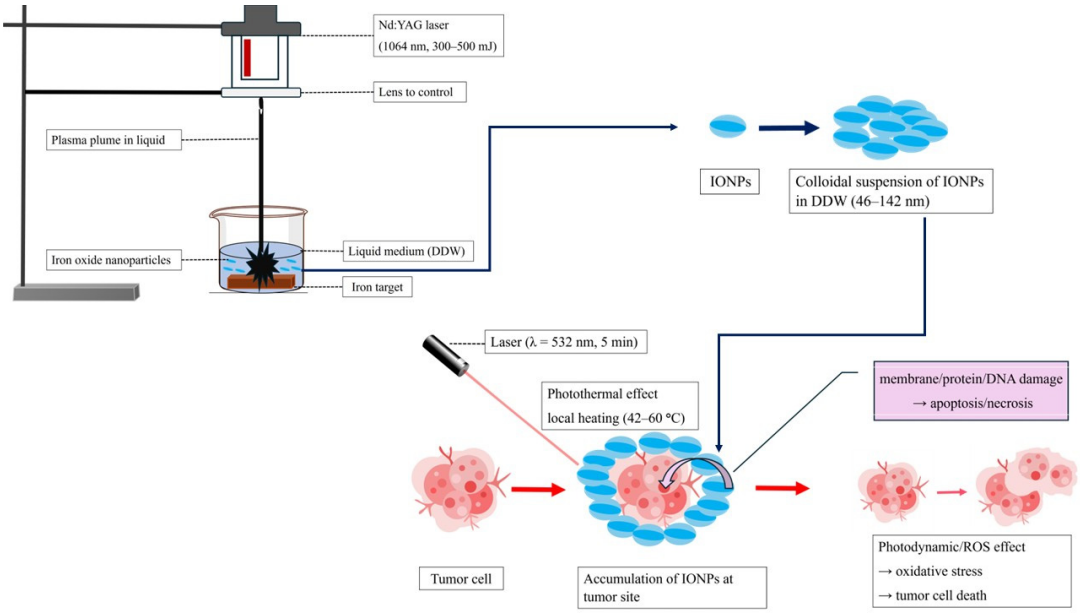

Fig. 1. Schematic of laser-ablated IONPs synthesis in water and their tumor-targeted photothermal/photodynamic effects under 532 nm irradiation, inducing oxidative stress and tumor cell death.

HepG2 cancer cells versus RD normal cells through crystal violet cytotoxicity assays, with and without 532 nm laser irradiation to demonstrate combined photothermal and photodynamic effects for targeted tumor therapy.

Experimental Section

Synthesis of IONPs

IONPs were synthesized via PLAL using a Q-switched Nd:YAG laser (λ = 1064 nm, pulse width = 10 ns, repetition rate = 1 Hz). A high-purity iron target (99%, 2 × 2 cm pellet, Sigma -Aldrich) was placed at the bottom of a glass vessel containing 3 mL double-distilled water (DDW) under constant magnetic stirring, and irradiated at laser energies of 300, 400, and 500 mJ per pulse for a fixed duration. A laser beam was focused on the target surface causing rapid warming, melting, and vaporization to generate a plasma plume, which expanded into the liquid medium, and then ultrafast quenching and interaction with dissolved oxygen facilitated the nucleation, growth and oxidation of iron species to IONPs, which consisted in a change of color to dark red colloid. Laser fluence was used to tune the particle size, concentration, and phase composition, higher energies gave rise to higher ablation rates and smaller and more crystalline nanoparticles.

Characterization Techniques

The phase composition, crystallinity, and size of the crystallites of the (IONPs) were determined through the X-ray diffraction (XRD; Shimadzu XRD-6000) analysis using Cu Kα radiation (λ = 1.5406 Å) at 2θ range of 20°–80° with a step size of 0.02 °and a scan rate of 5°/min. Phase identification was done against standard JCPDS databases through diffraction patterns.

Field emission scanning electron microscopy (FESEM; FEI NOVA NanoSEM450) was employed to examine nanoparticle morphology, shape, and size distribution.

Magnetic properties were evaluated using a vibrating sample magnetometer (VSM) at room temperature (300 K) over a field range of ±15 kOe, revealing size-, crystallinity-, and defect-dependent superparamagnetic behavior.

Anticancer activity

HepG2 (human hepatocellular carcinoma) cancer cells and RD (normal rhabdomyosarcoma) cells were independently cultured in 30 cm^2 flasks using RPMI-1640 medium supplemented with 10% fetal bovine serum (FBS) and incubated at 37°C in a humidified 5% CO_2 atmosphere for 24 h to reach 80–90% confluency prior to experiments.

Cytotoxicity assays

Cells were harvested from 25 cm^2 flasks by trypsin-EDTA detachment, neutralized with 20 mL serum-supplemented RPMI-1640, and resuspended. Aliquots (0.2 mL, ~10^4 cells/well) were seeded into 96-well flat-bottom plates in triplicate and incubated at 37°C, 5% CO_2 for 24 h to allow adherence. Medium was replaced with fresh medium containing IONPs at concentrations of 6.25, 12.5, 25, 50, and 100 μg/mL (three replicates per concentration), with untreated cell controls. After 24 h exposure ± 532 nm laser irradiation (5 min), viability was assessed by crystal violet assay: cells were fixed, stained (100 μL/well, 20 min), washed, destained, and absorbance measured at 492 nm using a microplate reader. Cytotoxicity (% inhibition) was calculated as:

Inhibition rate = (A – B) /A × 100 (1)

where A = mean OD of control wells and B = mean OD of IONP-treated wells.

Irradiation cancer cell by laser Diode

IONP-treated cells were irradiated using a 532 nm diode laser (5 min, tuned to nanoparticle absorption band) to activate photothermal and photodynamic effects. The laser induces: (i) photothermal heating via light absorption and conversion to localized hyperthermia (42–60°C), denaturing proteins, disrupting membranes/ DNA, and triggering apoptosis/necrosis; (ii) photodynamic ROS generation (- OH, O_2^-, $^1O_2$) through photoexcited electron transfer interacting with water/oxygen, causing oxidative stress, lipid peroxidation, mitochondrial dysfunction, and caspase-mediated cell death. Complementary mechanisms include magnetic guidance for tumor targeting, potential functionalization with antibodies/peptides/folic acid, vascular disruption, and immune activation via antigen release.

Statistical analysis

The statistical analysis of the results was conducted by using Graph Pad Prism Version 6 analysis software and analysis of variance. Means were compared by using the Duncan multiplex experiment, wherein significant differences were observed at a probability threshold of $P < 0.05$.

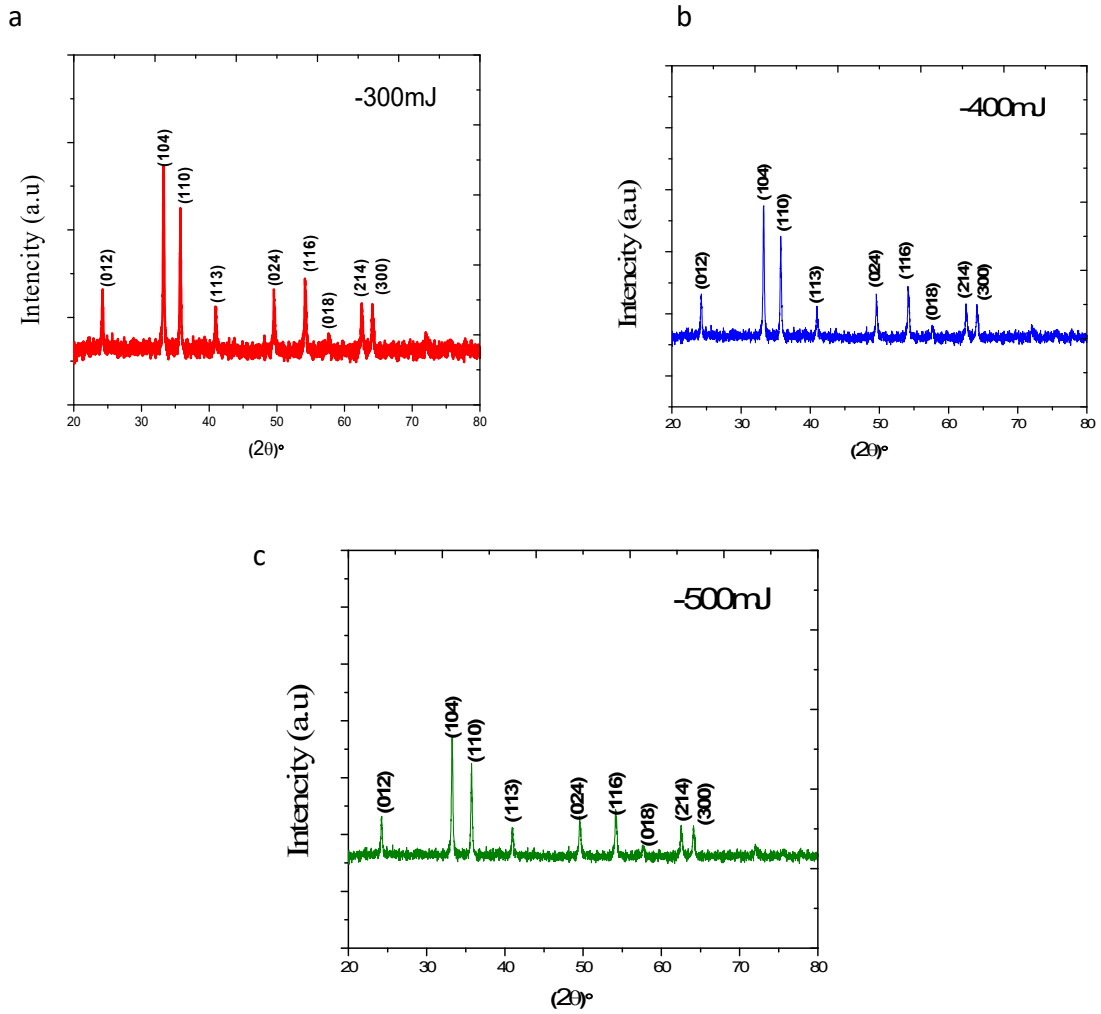

Fig. 2. XRD of Iron Oxide (a-300, b-400, c-500) mJ.

RESULTS AND DISCUSSION

Figure 2 presents XRD patterns of IONPs synthesized at laser energies of 300, 400, and 500 mJ, with 2θ (Bragg angle) on the x-axis and diffracted X-ray intensity (arbitrary units, a.u.) on the y-axis. Diffraction peaks, indexed with Miller indices (hkl), were identified by matching against the JCPDS reference for hematite. Peak intensity and sharpness increased with laser energy, indicating enhanced crystallinity and reduced lattice strain at higher fluences due to greater atomic mobility during nucleation. Broader peaks at 300 mJ suggest smaller crystallite sizes (~43 nm) or higher defect density, while narrower peaks at 500 mJ reflect improved crystallization (~33 nm) and potential preferred orientation, as evidenced by relative intensity variations across (hkl) planes.

Crystallite sizes were calculated using the Debye-Scherrer equation:

$$D = \frac{K\lambda}{\beta \cos\theta} \quad (2)$$

where DDD is the mean crystallite size, KKK = 0.94 (Scherrer constant), λ\lambdaλ = 1.5406 Å (Cu Kα wavelength), β\betaβ = peak full width at half maximum (FWHM, radians), and θ\thetaθ = Bragg angle. The most prominent peak yielded crystallite sizes of 43 nm (300 mJ), 40 nm (400 mJ), and 33 nm (500 mJ), confirming energy-dependent refinement of nanoparticle crystallinity.

Fig. 3 of the FESEM depicts irregular, agglomerated nanoparticles whereby the primary particles are mostly spherical with a few polyhedral ones forming clusters probably through van der

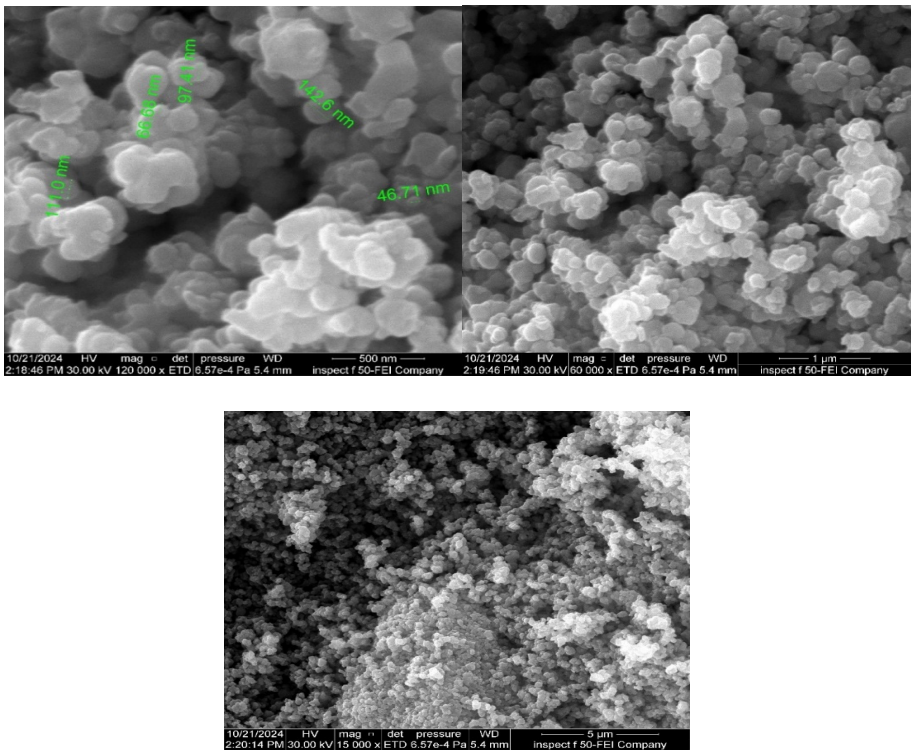

Fig.3. FESEM images of IONPs.

Waals attractions and/or partial sintering.

At 500 mJ, the higher laser energy enhances ablation and plasma formation, increasing fragmentation and nucleation rates and thus favoring the generation of smaller nanoparticles while inhibiting secondary growth and aggregation through stronger repulsive interactions. In contrast, at 300–400 mJ, reduced ablation efficiency and lower thermal input lead to incomplete fragmentation, slower nucleation and growth, and consequently larger particles with a higher tendency to aggregate. Overall, the measured particle diameters range from about 46 to 142 nm, indicating a polydisperse system in which the smaller nanoparticles likely represent primary particles, whereas the larger ones are aggregates or agglomerates[7, 25].

Laser-induced heating can reduce the size of IONPs, and when the particle size falls below about 20 nm the system can exhibit superparamagnetic behavior characterized by a narrow hysteresis loop and reduced coercivity (Hc), as observed for the smaller particles produced at 500 and 400 mJ in Fig. 4. In addition, higher laser energies may introduce lattice defects, strain, or oxygen vacancies in the IONPs, which can modify their magnetic properties, often enhance the saturation magnetization (Ms) and alter Hc. Conversely, at 300 mJ the larger particles show higher coercivity and a wider hysteresis loop consistent with more stable ferromagnetic-like behavior, while a different defect structure at this lower energy may contribute to the observed decrease in Ms

The optical spectra of IONPs samples prepared by laser ablation at 300, 400, and 500 mJ (Fig. 5) show that the absorbance decreases with increasing wavelength, with noticeably higher absorption in the short-wavelength region, which can be attributed to electronic transitions from the valence band to the conduction band and is consistent with a nanostructured material. In addition, the sample produced at the highest laser energy exhibits the greatest overall absorbance, implying more efficient vaporization of the IONPs target, a higher nanoparticle concentration, and likely smaller or more densely packed nanoparticles that provide more light-absorbing active sites. This enhanced absorption can be associated with size-dependent effects such as surface plasmon resonance or quantum confinement in the nanoscale regime, which are known to increase the optical response of metal oxide nanoparticles.

Two cell lines, the hepatocellular carcinoma cell

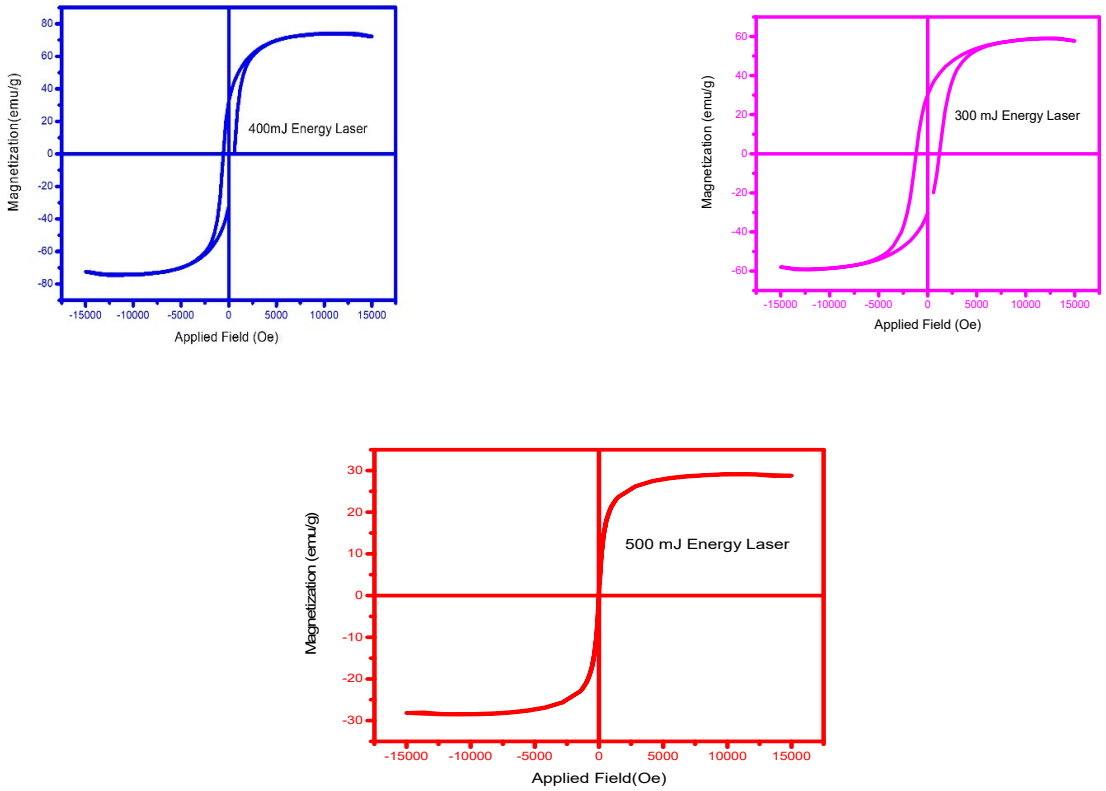

Fig. 4. VSM of Iron Oxide (a-300 purple, b-400 blue, c-500 red) mJ.

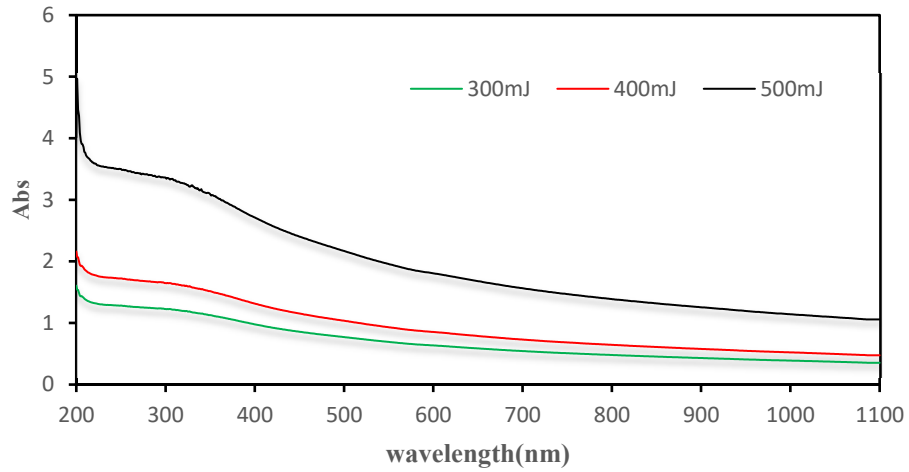

Fig. 5. Optical properties of IONPs at various laser energies (300, 400, and 500 mJ)

line HepG2 and the normal muscle cell line RD, were treated with IONPs at concentrations of 6.25, 12.5, 25, 50, and 100 µg/ml and irradiated with a 532 nm laser diode for 5 min, then incubated for 24 h at 37 °C. The viability data (Tables 1 and 2) show a clear concentration-dependent inhibitory effect of IONPs on both HepG2 and RD cells after 24 h, with the strongest cytotoxicity observed for nanoparticles synthesized at 500 mJ, which likely reflects their higher concentration in the colloid and smaller size, and thus larger specific surface area, compared with particles produced at 300 and 400 mJ. In line with previous reports [26-29], on laser-ablated iron oxide nanomaterials, the

Table 1. Inhabitation rates on the normal RD cell line under the effect of different concentrations of (IONPs µg/ml) after irradiation by laser diode 532 nm.

NO	concentrations (µg/ml)	Inhabitation (%)
1	6.25	0
2	12.5	0
3	25	0
4	50	15.11
5	100	19.22

Table 2. Inhibition rates in the normal HepG2 cell line due to different concentrations of (IONPs µg/ml) after irradiation by laser diode 532 nm.

Concentration (µg/ml)	Inhabitation (%) of IONPs (500 mJ)	Inhabitation (%) of IONPs (400 mJ)	Inhabitation (%) of IONPs (300 mJ)
6.25	29.86	24.87	22.07
12.5	43.41	49.98	46.45
25	49.31	51.11	59.42
50	53.32	68.92	73.32
100	66.10	80.31	86.67

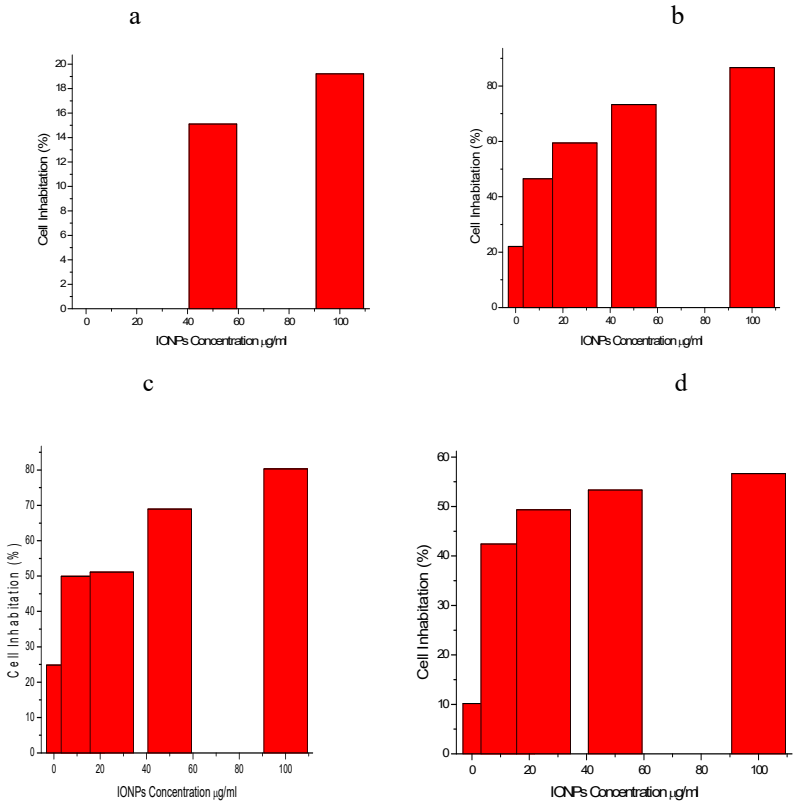

Fig. 6. Ablation method used energies: a. 300 mJ for normal cells(b.300 mJ, c. 400 and d. 500mJ cancer cells).

increased surface area and reactivity of smaller IONPs enhance their interaction with cells and consequently their inhibitory potential on cell proliferation. Furthermore, Fig. 6 illustrates that laser-activated IONPs can act as targeted therapeutic agents, where their magnetic and photothermal/photodynamic responses promote localized heating, reactive oxygen species generation, mitochondrial dysfunction, and ultimately apoptosis in tumor cells, thereby improving tumor damage while potentially limiting systemic toxicity, consistent with earlier studies

[30-33] on IONP-mediated cancer therapy.

CONCLUSION

The synthesis of IONPs by laser ablation represents a green and efficient route for producing high-purity colloids without chemical precursors or stabilizing agents. XRD analysis in this work confirms the formation of iron oxide phases under the applied ablation conditions, while FESEM images show nearly spherical nanoparticles in the nanometer range whose size can be tuned by adjusting laser energy, pulse characteristics, and wavelength. The combination of favorable biocompatibility and magnetic behavior makes such IONPs attractive for biomedical use, including magnetic hyperthermia, targeted delivery, and MRI contrast enhancement, where superparamagnetic-like responses are particularly advantageous. The data in the cytotoxicity results show that the particles have the capacity to selectively induce apoptosis in cancer cells and relatively less effect on normal cells, which suggest their potential use as anticancer applications. Altogether, laser ablation is the clean and controllable method of preparing iron oxide nanoparticles to be used in cancer treatment, and further research needs to refine the size control and surface functionalization of particles and extensive in vivo tests to bring the potential of these nanoparticles to full realization, according to the current development trends in nanomedicine.

ACKNOWLEDGEMENT

The authors utilized artificial intelligence tools, namely Perplexity.ai, to enhance the clarity and language quality of this manuscript throughout its preparation. All suggestions and content provided by the AI were thoroughly reviewed and revised by the authors, who take full responsibility for the accuracy and integrity of the final version.

CONFLICT OF INTEREST

The authors declare no conflict of interest.

REFERENCES

1. Sportelli, M.C., et al., The pros and cons of the use of laser ablation synthesis for the production of silver nano-antimicrobials. Antibiotics, 2018. 7(3): p. 67. https://doi.org/10.3390/antibiotics7030067
2. Balachandran, A., et al., Nanoparticle production via laser ablation synthesis in solution method and printed electronic application-A brief review. Results in Engineering, 2022. 16: p. 100646. https://doi.org/10.1016/j.rineng.2022.100646
3. Kim, M., et al., Synthesis of nanoparticles by laser ablation: A review. KONA Powder and Particle Journal, 2017. 34: p. 80-90. https://doi.org/10.14356/kona.2017009
4. Domínguez-Crespo, M., et al., Production of BN nanostructures by pulsed laser ablation in liquids: influence of the applied Nd: YAG harmonics on the structural, optical and photoluminescence properties. Ceramics International, 2020. 46(13): p. 21667-21680. https://doi.org/10.1016/j.ceramint.2020.05.274
5. Amendola, V. and M. Meneghetti, Laser ablation synthesis in solution and size manipulation of noble metal nanoparticles. Physical chemistry chemical physics, 2009. 11(20): p. 3805-3821. https://doi.org/10.1039/b900654k
6. Kabashin, A.V. and V.Y. Timoshenko, What theranostic applications could ultrapure laser-synthesized Si nanoparticles have in cancer? 2016, Taylor & Francis. p. 2247-2250. https://doi.org/10.2217/nnm-2016-0228
7. Fazio, E., et al., Nanoparticles engineering by pulsed laser ablation in liquids: Concepts and applications. Nanomaterials, 2020. 10(11): p. 2317. https://doi.org/10.3390/nano10112317
8. Dell'Aglio, M., et al., Mechanisms and processes of pulsed laser ablation in liquids during nanoparticle production. Applied Surface Science, 2015. 348: p. 4-9. https://doi.org/10.1016/j.apsusc.2015.01.082
9. Fromme, T., et al., Laser synthesis of nanoparticles in organic solvents - products, reactions, and perspectives. Beilstein Journal of Nanotechnology, 2024. 15: p. 638-663. https://doi.org/10.3762/bjnano.15.54
10. Yang, C., S. Li, and L. Wang, Engineered iron oxide nanoplatforms: reprogramming immunosuppressive niches for precision cancer theranostics. Molecular Cancer, 2025. 24(1): p. 225. https://doi.org/10.1186/s12943-025-02443-2
11. Soetaert, F., et al., Cancer therapy with iron oxide nanoparticles: Agents of thermal and immune therapies. Advanced drug delivery reviews, 2020. 163: p. 65-83. https://doi.org/10.1016/j.addr.2020.06.025
12. Shestovskaya, M.V., et al., Iron oxide nanoparticles in cancer treatment: cell responses and the potency to improve radiosensitivity. Pharmaceutics, 2023. 15(10): p. 2406. https://doi.org/10.3390/pharmaceutics15102406
13. Rajan, A., et al., Recent advancements and clinical aspects of engineered iron oxide nanoplatforms for magnetic hyperthermia-induced cancer therapy. Materials Today Bio, 2024. 29: p. 101348. https://doi.org/10.1016/j.mtbio.2024.101348
14. Mandal, S., Revolutionizing Oncology: Iron Oxide Nanoparticles in Cancer Diagnosis and Treatment. International Journal of Scientific Research in Science and Technology, 2025. 12(1): p. 161-173. https://doi.org/10.32628/IJSRST2512126
15. Horvat, N.K., et al., Superparamagnetic iron oxide nanoparticles reprogram the tumor microenvironment and reduce lung cancer regrowth after crizotinib treatment. ACS nano, 2024. 18(17): p. 11025-11041. https://doi.org/10.1021/acsnano.3c08335
16. Maneeratanasarn, P., et al., Synthesis of phase-controlled iron oxide nanoparticles by pulsed laser ablation in different liquid media. physica status solidi (a), 2013. 210(3): p. 563-569. https://doi.org/10.1002/pssa.201228427
17. Rivera-Chaverra, M.J., et al., Synthesis of oxide iron nanoparticles using laser ablation for possible hyperthermia applications. Nanomaterials, 2020. 10(11): p. 2099. https://doi.org/10.3390/nano10112099
18. Espinosa, A., et al., Duality of iron oxide nanoparticles

in cancer therapy: amplification of heating efficiency by magnetic hyperthermia and photothermal bimodal treatment. ACS nano, 2016. 10(2): p. 2436-2446. https://doi.org/10.1021/acsnano.5b07249
19. Estelrich, J. and M.A. Busquets, Iron oxide nanoparticles in photothermal therapy. Molecules, 2018. 23(7): p. 1567. https://doi.org/10.3390/molecules23071567
20. Yao, H. and J.-Y. Zhou, Chlorin e6-modified iron oxide nanoparticles for photothermal-photodynamic ablation of glioblastoma cells. Frontiers in Bioengineering and Biotechnology, 2023. 11: p. 1248283. https://doi.org/10.3389/fbioe.2023.1248283
21. Wang, D., et al., Targeted iron-oxide nanoparticle for photodynamic therapy and imaging of head and neck cancer. ACS nano, 2014. 8(7): p. 6620-6632. https://doi.org/10.1021/nn501652j
22. Zhi, D., et al., Targeting strategies for superparamagnetic iron oxide nanoparticles in cancer therapy. Acta biomaterialia, 2020. 102: p. 13-34. https://doi.org/10.1016/j.actbio.2019.11.027
23. Palanisamy, S. and Y.-M. Wang, Superparamagnetic iron oxide nanoparticulate system: synthesis, targeting, drug delivery and therapy in cancer. Dalton transactions, 2019. 48(26): p. 9490-9515. https://doi.org/10.1039/C9DT00459A
24. Janko, C., et al., Functionalized superparamagnetic iron oxide nanoparticles (SPIONs) as platform for the targeted multimodal tumor therapy. Frontiers in oncology, 2019. 9: p. 59. https://doi.org/10.3389/fonc.2019.00059
25. Lee, B.H.-j. and G. Arya, Analytical van der Waals interaction potential for faceted nanoparticles. Nanoscale Horizons, 2020. 5(12): p. 1628-1642. https://doi.org/10.1039/D0NH00526F
26. Jabbar, M.S., et al., Synthesis and Characterization of TiO2-CQDs Nanocomposites and Testing of Their Anticancer Potential. International Journal of Nanoelectronics and Materials (IJNeaM), 2024. 17(4): p. 627-633. https://doi.org/10.58915/ijneam.v17i4.1383
27. Adamczyk-Grochala, J., et al., Evaluation of anticancer activity of urotropine surface modified iron oxide nanoparticles using a panel of forty breast cancer cell lines. Nanotoxicology, 2025: p. 1-19. https://doi.org/10.1080/17435390.2025.2450196
28. Tabbasum MD, T. and Sridharan, In Vitro and In Silico Analysis of Iron Oxide Nanoparticles from Anastatica hierochuntica. BioNanoScience, 2025. 15(1): p. 4. https://doi.org/10.1007/s12668-024-01700-w
29. Taudul, J., et al., Tailored Iron Oxide Nanoparticles as Potential Cannabinoid Carriers for Anti-Cancer Treatment. Biomolecules, 2025. 15(2): p. 230. https://doi.org/10.3390/biom15020230
30. Parmanik, A. and A. Bose, Targeted anticancer drug delivery via surface engineered iron oxide nanoparticles: A recent update. Journal of Drug Delivery Science and Technology, 2023. 90: p. 105120. https://doi.org/10.1016/j.jddst.2023.105120
31. Shah, A., et al., Synthesis of Iron Oxide Nanoparticles and its Antimicrobial, Anticancer, Anti-inflammatory, Wound Healing, and Immunomodulatory Activities-A Review. Phytopharmacology Research Journal, 2024. 3(3): p. 1-28.
32. Navya, H., et al., Eco-friendly Synthesis of Iron Oxide Nanoparticles (IO-NPs) from aqueous extract of Cissus quadrangularis L.(Veld grape): Characterization and Pharmaceutical Evaluation. Journal of Molecular Structure, 2025: p. 141685. https://doi.org/10.1016/j.molstruc.2025.141685
33. Udupi, A., et al., Anticancer therapeutic potential of multimodal targeting agent-"phosphorylated galactosylated chitosan coated magnetic nanoparticles" against N-nitrosodiethylamine-induced hepatocellular carcinoma. Drug Delivery and Translational Research, 2025. 15(3): p. 1023-1042. https://doi.org/10.1007/s13346-024-01655-1